Visible Photocatalytic Activity Enhancement of ZnWO$_4$ by Graphene Hybridization

Xiaojuan Bai, Li Wang, and Yongfa Zhu*

Department of Chemistry, Tsinghua University, Beijing 10084, People's Republic of China

S *Supporting Information*

ABSTRACT: ZnWO$_4$/graphene hybride (GZW-X) photocatalysts were synthesized via a facile in situ reduction of graphene oxide and ZnWO$_4$ in water. High efficiency for the degradation of methylene blue (MB) under both UV light and visible light was obtained for the GZW-X photocatalysts. The photocatalytic efficiency of ZnWO$_4$/graphene-0.2 wt % under visible-light and UV-light irradiation was ~7.1 and 2.3 times that of pristine ZnWO$_4$, respectively. The visible photocatalytic activity originated from the $^\bullet$OH and O$_2^{\bullet-}$, which were formed by photosensitization of graphene in ZnWO$_4$/graphene. The enhancement of UV photocatalytic light activity in ZnWO$_4$/graphene was attributed to the high separation efficiency of photoinduced electron−hole pairs resulting from the promotion of HOMO orbit of graphene in ZnWO$_4$/graphene.

KEYWORDS: photocatalysis, ZnWO$_4$, graphene, hybridization
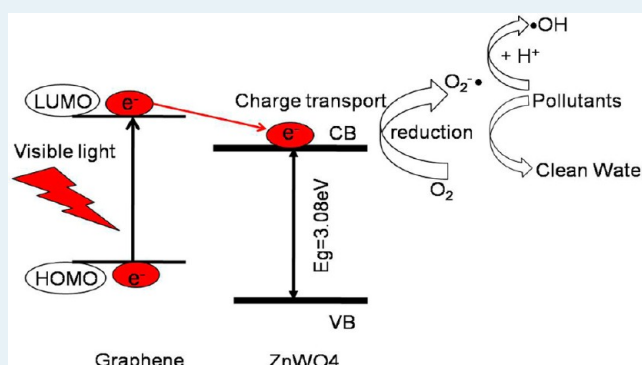
INTRODUCTION

Photocatalytic degradation of organic pollutants by semiconductor photocatalysts is promising for environmental purification and energy conversion.[1−5] As an important photocatalyst, ZnWO$_4$ has been applied for photocatalytic production of hydrogen from water and mineralization of organic pollutants under UV light irradiation.[6−8] Since the first successful preparation of ZnWO$_4$,[9] several studies have extended new routes to synthesize ZnWO$_4$-based photocatalysts. In recent years, our group has made many efforts on ZnWO$_4$, such as to enhance the activity by tuning morphologies,[10] controlling crystallinity,[11,12] and ion doping,[13,14] or to explore the photoelectrocatalytic activies.[15] Recently, He et al. prepared several ZnWO$_4$-based composites of high UV light photocatalytic activities via facile hydrothermal methods.[16] Meanwhile, Sun et al. predicted the enhanced photoactivity of ZnWO$_4$ by C, N, and F pairwise codoping according to first-principles density function theory calculations.[17] In all of these cases, ZnWO$_4$ photocatalysts present no visible light photocatalytic activity because of the large band gap (3.2 eV). However, visible-light-responsive ZnWO$_4$ photocatalysts are highly desired from the viewpoint of utilizing solar light. Although nonmetal doping—in particular, fluorine doping[13]—shows great potential in enhancing photocatalytic activity, it is still challenging to make ZnWO$_4$ visible light photocatalytically active.

On the other hand, a hybridized semiconductor with a conjugative π structure material has been proved to be effective for enhancing photocatalytic activity; for example, C$_{60}$−ZnO,[18] polyaniline−TiO$_2$,[19] graphite-like carbon (e.g., C$_3$N$_4$) hybri-dized ZnO[20]/Bi$_2$WO$_6$[21] all present higher photocatalytic activity than the pristine. Wang et al. reported a one-step solvothermal synthesis of a carbon@TiO$_2$ dyade structure effectively promoting visible light photocatalysis. They showed for the first time that the surface of nanometer-sized carbon materials can also show collective polarization modes, and these optical absorption transitions are feasible to sensitize TiO$_2$, which then acts as a novel "dyade"-type structure.[22] They also demonstrated an effective approach for the fabrication of graphene-based carbon nitride nanosheets as efficient metal-free electrocatalysts for oxygen reduction reactions.[23]

Xu et al. consider that TiO$_2$−GR is, in essence, the same as other TiO$_2$−carbon (carbon nanotubes, fullerenes, and activated carbon) composite materials on enhancement of the photocatalytic activity of TiO$_2$.[24] Graphene behaves as a conjugative π structure[25,26] and large specific surface area, so it is promising for enhancing photocatalytic activity in terms of a strong adsorptivity of pollutants, high absorption, long electron−hole pair lifetimes, and an extended light absorption range.[27]

The interaction between graphene and a photocatalyst in nanocomposites was reported in photocatalytic and optoelectronic systems. Williams et al. developed a UV-assisted photocatalytic reduction of graphene oxide in a TiO$_2$−graphene system. The binding of the oxide particles keeps the exfoliated graphene sheets from collapsing after the reduction step. The

method offers a new and soft method of reduction as compared to the conventional approach of using elevated temperatures or strong reducing agents for reducing graphene oxides.[28] They also demonstrated excited-state interactions existed between ZnO nanoparticles and graphene oxide. Graphene oxide sheets suspended in ethanol interact with excited ZnO nanoparticles and undergo photocatalytic reduction.

Anchoring of ZnO nanoparticles on 2D carbon nanostructures provides a new way to design carbon−semiconductor nanocomposites for catalytic applications.[29] Lee et al. report ZnO nanorod−graphene hybrid architectures (ZnO−GHAs) composed of regular arrays of ZnO nanorods formed on few-layer graphene films transferred to transparent or flexible substrates. The material can be applicable for next-generation electronic and optoelectronic systems.[30] Graphene-based photocatalytists are have been demonstrated to be very efficient in photocatalytic production of hydrogen from water and mineralization of organic pollutants.[31,32] Li et al. confirmed that a P25-graphene nanocomposite prepared via a facile one-step hydrothermal exhibited UV and visible photocatalytic activity that was superior to pristine P25 in the photodegradation of MB by utilizing the large specific surface area and charge transportation of graphene.[33]

It has been reported by Fu and Wang that a $ZnFe_2O_4$−graphene nanocomposite showed enhanced visible photocatalytic activity over pristine $ZnFe_2O_4$ in the presence of H_2O_2. The significant enhancement in photoactivity is ascribed to the efficient separation of photogenerated carriers in the $ZnFe_2O_4$ and graphene coupling system and the concerted effects of individual components or their integrated properties[34] Amal and co-workers found that the visible-light-induced water splitting catalyzed by $BiVO_4$ was enhanced by graphene. This improvement is attributed to the longer electron lifetime of excited $BiVO_4$ as the electrons are injected to graphene instantly at the site of generation, leading to a minimized charge recombination.[35] Xu et al. demonstrated ZnO/graphene nanocomposites exhibited a higher UV light photocatalytic activity than pristine ZnO by taking advantage of the superior electrical conductivity and mechanical properties of graphene.[36]

To enhance the photocatalytic activity, there have been persistent efforts to load photocatalysts on the structure of graphene, but few studies have focused on the surface coating by graphene on the photocatalyst for enhancing the photocatalytic efficiency and producing visible photocatalytic activity. Therefore, in this work, the surface coating structure of graphene on $ZnWO_4$ as well as the hybridized mechanism of enhanced photocatalytic efficiency and produced visible photocatalytic activity were vigorously studied.

Herein, a facile route to synthesize the visible-light-responsive graphene hybridized $ZnWO_4$ nanorods was developed. Furthermore, the UV activity was enhanced, and visible light activity was produced after $ZnWO_4$ nanorods were hybridized by graphene. To the best of our knowledge, this is the first report on visible light photoactivity of graphene hybridized $ZnWO_4$. The synergic effect between $ZnWO_4$ and graphene and the possible mechanisms of enhancement of photocatalytic activity were systematically investigated.

■ EXPERIMENTAL SECTION

Materials. Titanium dioxide (TiO_2) nanopowder is the commercial P25 (Degussa Co., Ltd., Germany). Graphene oxide (GO) was synthesized by the modified Hummmers' method,[37] and graphene was prepared according to the

literature.[38] All chemicals were analytical reagent grade and were used without further purification.

Synthesis of $ZnWO_4$. $ZnWO_4$ was prepared by hydrothermal synthesis according to the literature.[6] The details are as follows: 0.001 mol of $Na_2WO_4 \cdot 2H_2O$ and 0.001 mol of $Zn(NO_3)_2$ were added to 15 mL of deionized water with magnetic stirring to form a homogeneous solution. The solution pH was adjusted to 11 using 0.5 M NaOH. The mixture was then sealed in a 50 mL Teflon-lined stainless steel autoclave and was heated at 180 °C for 24 h. After cooling, the product was filtered, washed, and dried at 60 °C for 10 h.

Sample Preparation. A certain amount of GO was dispersed in water, then exfoliation of graphene oxide was achieved by ultrasonicating the dispersion for 60 min. The obtained brown dispersion was then subjected to centrifugation to remove the unexfoliated GO. The obtained exfoliated GO was then dispersed in 100 mL water, and the as-prepared $ZnWO_4$ was added into the dispersion and dispersed by ultrasonication for 30 min and stirred for 48 h. The reduction of GO to graphene was performed according to the literature.[39] In a typical procedure, an appropriate amount of hydrazine solution (35 wt % in water) and ammonia solution (28 wt % in water) were added to the above dispersion. After being vigorously stirred for a few minutes, the dispersion was put into a water bath (90 °C) for 3 h. An opaque powder was obtained after evaporation at 60 °C for 12 h. $ZnWO_4$/graphene composites with different mass ratios ranging from 0.004% to 2.0% were prepared according to this method. The $ZnWO_4$/graphene-X wt % composite photocatalysts were marked as GZW-X, X label as graphene/$ZnWO_4$ mass ratio 0.004, 0.02, 0.05, 0.2, 0.8, 2.0. The $ZnWO_4$/graphene mixture−0.2 wt % was marked as GMW0.2.

$ZnWO_4$ and $ZnWO_4$/graphene electrodes were prepared as follows: 4 mg of as-prepared photocatalyst was suspended in 2 mL of ethanol to produce a slurry, which was then dip-coated onto a 2 cm × 4 cm indium−tin oxide (ITO) glass electrode. Electrodes were exposed to UV light for 10 h to remove ethanol and subsequently calcined at 180 °C for 10 h under N_2 flow (rate = 60 mL/min). All investigated electrodes were of similar thickness (0.8−1.0 μm).

Characterizations. High-resolution transmission electron microscopy (HRTEM) images were obtained by a JEOL JEM-2011F field emission transmission electron microscope with an accelerating voltage of 200 kV. To avoid electron beam-induced damage, a low-intensity beam was used for collecting selected area electron diffraction patterns. X-ray diffraction (XRD) patterns of the powders were recorded at room temperature by a Bruker D8 Advance X-ray diffractometer. The diffuse reflectance absorption spectra of the samples were recorded in the range from 250 to 800 nm using a Hitachi U-3010 spectroscope equipped with an integrated sphere attachment, and $BaSO_4$ was used as a reference. Raman spectra were recorded on a microscopic confocal Raman spectrometer (Renishaw 1000 NR) with an excitation of 514.5 nm laser light. Fourier transform infrared (FTIR) spectra were carried out using a Perkin-Elmer spectrometer in the frequency range of $4000-450$ cm^{-1} with a resolution of 4 cm^{-1}. X-ray photoelectron spectroscopy (XPS) was measured in a PHI 5300 ESCA system. The beam voltage was 3.0 kV, and the energy of the Ar ion beam was 1.0 keV. The binding energies were normalized to the signal for adventitious carbon at 284.8 eV. The Brunauer−Emmett−Teller (BET) surface area measurements were performed by a micromeritics (ASAP 2010
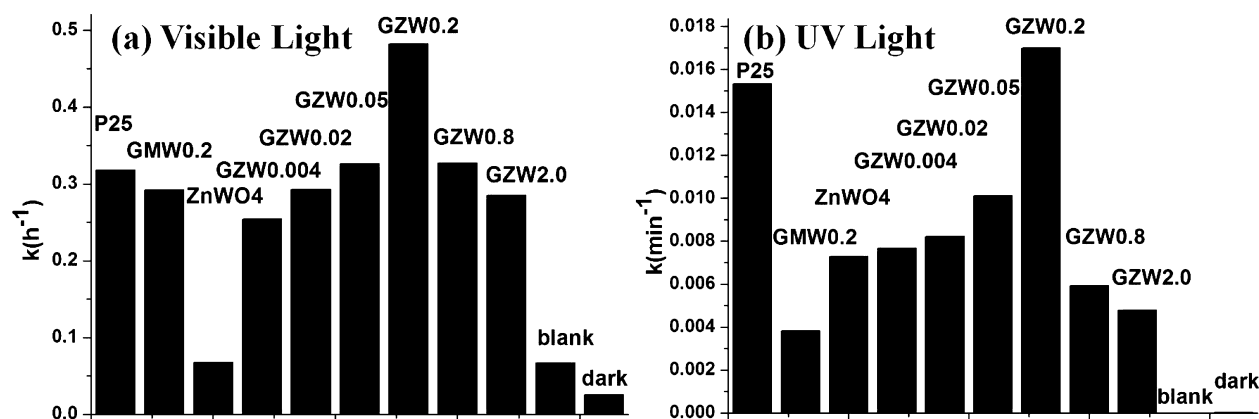
Figure 1. Apparent rate constants for the photodegradation of MB over $ZnWO_4$ and $ZnWO_4$/graphene photocatalysts (a) under visible light irradiation ($\lambda > 420$ nm, [MB] = 0.01 mM) and (b) under UV light irradiation ($\lambda = 254$ nm, [MB] = 0.03 mM).

V5.02H) surface area analyzer. The nitrogen adsorption and desorption isotherms were measured at 77 K after degassing the samples on a Sorptomatic 1900 Carlo Erba instrument. The electron spin resonance (ESR) signals of radicals spin-trapped by spin-trap reagent 5,5′-dimethyl-1-pirroline-N-oxide (DMPO) (purchased from Sigma Chemical Co.) were examined on a Bruker model ESR JES-FA200 spectrometer equipped with a quanta-Ray Nd:YAG laser system as the irradiation source ($\lambda = 365/420$ nm). To minimize experimental errors, the same type of quartz capillary tube was used for all ESR measurements. The ESR spectrometer was coupled to a computer for data acquisition and instrument control. Magnetic parameters of the radicals detected were obtained from direct measurements of magnetic field and microwave frequency. Electrochemical and photoelectrochemical measurements were performed in three-electrode quartz cells with a 0.1 M Na_2SO_4 electrolyte solution. Platinum wire was used as the counter electrode, and saturated calomel electrodes (SCE) were used as the reference electrodes, respectively. $ZnWO_4$ and $ZnWO_4$/graphene film electrodes on ITO served as the working electrode. The photoelectrochemical experiment results were recorded using an electrochemical system (CHI-660B, China). The intensity of light was 1 mW/cm². Potentials are given with reference to the SCE. The photoresponses of the photocatalysts as UV light on and off were measured at 0.0 V. Electrochemical impedance spectra (EIS) were measured at 0.0 V. A sinusoidal ac perturbation of 5 mV was applied to the electrode over the frequency range of $0.05-10^5$ Hz.

Photocatalytic Experiments. The photocatalytic activities were evaluated by the decomposition of methylene blue (MB) under UV light ($\lambda = 254$ nm, 11 W) and visible light irradiation ($\lambda > 420$ nm). Visible irradiation was obtained from a 500 W xenon lamp (Institute for Electric Light Sources, Beijing) with a 420 nm cutoff filter, and the average visible light intensity was 38 mW/cm². A 50 mg portion of photocatalyst was totally dispersed in an aqueous solution of MB (100 mL, 0.03 mM for UV light; 0.01 mM for visible light;). Before irradiation, the suspensions were magnetically stirred in the dark for 60 min to get absorption−desorption equilibrium between the photocatalyst and MB. At certain time intervals, 5 mL aliquots were sampled and centrifuged to remove the particles. The concentration of the MB was analyzed by recording the absorbance at the characteristic band of 663 nm using a Hitachi U-3010 UV−vis spectrophotometer.

RESULTS AND DISCUSSION

Photocatalytic Activity and Photocurrent Response. The photocatalytic activities of the as-prepared samples for the degradation of methylene blue (MB) in solution were tested under visible light and UV light irradiation. The results are shown in Figure 1a and b, respectively. The photocatalytic degradation of organic pollutants generally follows pesudo-first-order kinetics. As shown in Figure 1a, $ZnWO_4$/graphene photocatalysts present visible light photocatalytic activity obviously superior to that of the pristine $ZnWO_4$. Since the little degradation of MB over pristine $ZnWO_4$ may be attibuted to the natural photolysis, $ZnWO_4$, in fact, shows no visible photocatalytic activity. However, $ZnWO_4$/graphene-0.2 wt % (GZW0.2) achieved 92% degradation of MB in 5 h under visible light irradiation, which is ~1.2 times that of the physical mixture $ZnWO_4$/graphene mixture-0.2 wt % (GMW0.2). This result suggests the chemical contact may exist between $ZnWO_4$ and graphene, which is possibly the interelectron transfer at the interface.

Figure 1b shows the MB degradation rate constants over $ZnWO_4$ and $ZnWO_4$/graphene under UV light irradiation. The photocatalytic activity of $ZnWO_4$/graphene increases gradually with an increasing proportion of graphene and reaches the optimum activity when the proportion of graphene reaches to 0.2 wt %. The highest apparent rate constant of $ZnWO_4$/graphene is 0.017 min⁻¹, which is 2.3 times that of pristine $ZnWO_4$. A further increase in the graphene content leads to a significant decrease in photocatalytic activity, which may be attributed to increased absorbance and scattering of photons through excess graphene in the photosystem.[36] Thus, to achieve an optimal photocatalytic performance, it is crucial to control the composition ratio in $ZnWO_4$/graphene nanocomposite. In the case of different potocatalysts, as shown in Figure 1b, the photodegradation efficiency follows the order GZW0.2 > P25 > $ZnWO_4$ > GMW0.2. Therefore, the hybridization of graphene could both enhance the UV light photocatalytic activity and induce the considerable visible light photocatalytic activity of the $ZnWO_4$, indicating a possible synergetic effect between graphene and $ZnWO_4$.

To confirm the photocatalytic process, blank tests were performed, as shown in Figure 1a, b. No obvious degradation of MB is observed in the dark in the presence of the catalyst, and only a weak photolysis of MB can be observed under visible light and UV light in the absence of photocatalysts, confirming the considerable photocatalytic activity of $ZnWO_4$/graphene.
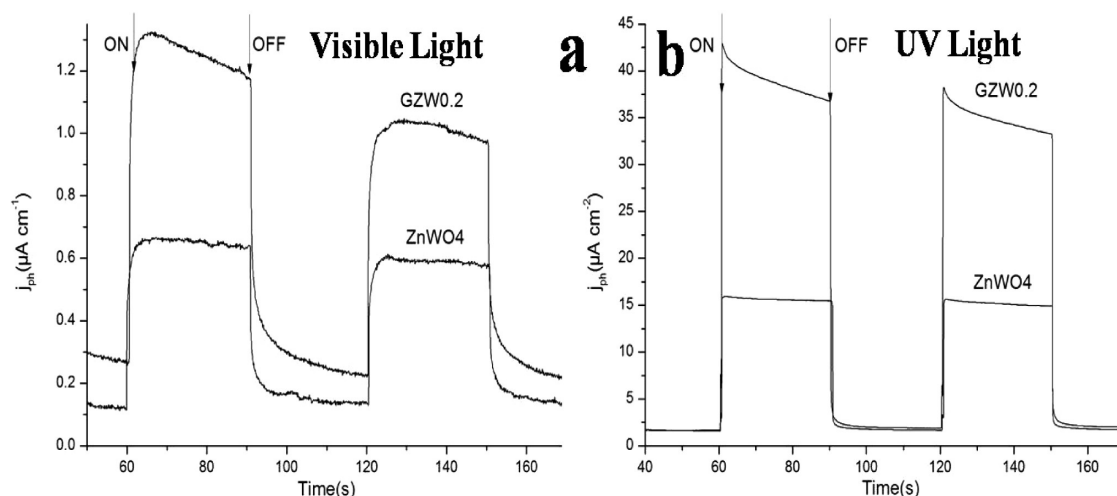
Figure 2. The transient photocurrent density responses of $ZnWO_4$ and GZW0.2 electrodes with light on/off cycles: (a) under visible light irradiation ($\lambda > 420$ nm) and (b) under UV light irradiation ($\lambda = 254$ nm, $[Na_2SO_4] = 0.1$ M).
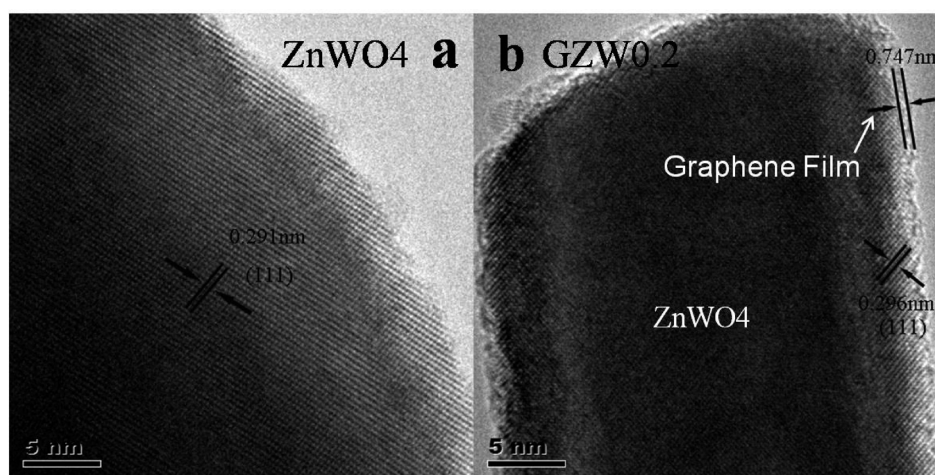

Figure 3. HRTEM images of $ZnWO_4$ and GZW0.2 photocatalysts (a) $ZnWO_4$ and (b) GZW0.2.

Figure 2a, b shows the transient photocurrent responses via two on−off cycles of $ZnWO_4$ and $ZnWO_4$/graphene electrodes under visible and UV light irradiation, which may directly correlate with the recombination efficiency of the photo-generated carriers.[40−42] As shown in Figure 2a, b, a generation of photocurrent with good reproducibility for all samples is observed when samples are irradiated by visible and UV light. This indicates that the electrode is stable and the photo-response is quite reversible. The visible- and UV-irradiated photocurrent densities of $ZnWO_4$/graphene-0.2 wt % (GZW0.2) are 2.2 and 2.3 times that of pristine $ZnWO_4$, respectively. This photocurrent efficiency is very consistent with photocatalytic activities. Thus, in the case of GZW0.2, the separation and transfer of photoinduced electron−hole pairs are more efficient due to the interfacial interaction between graphene and $ZnWO_4$.[20,21]

It was recently reported that the carbon of graphene can be consumed in the photocatalytic process, but graphene in these system is based on physical adsorption or loaded.[43−49] A monolayer hybrid effect, the chemical interaction between graphene and photocatalysts, was demonstrated to be stable, such as C_{60},[18] C_3N_4,[20,21] and polyaniline.[19] However, polyani-line of a multilayer physical adsorption would be photo-

degraded until only monolayer polyaniline remained.[19] In this work, the strong hybrid effect for the $ZnWO_4$/graphene system emerged on the interface in the monolayer of graphene. The results of the photostability experiment show that the photocatalytic activity of GZW0.2 exhibits only a 0.7% decrease after running for five cycles (about 20 h of irradiation), indicating that GZW0.2 is a stable visible light photocatalyst and graphene is not a sacrificial reactant in the photocatalytic reaction (Supporting Information Figure S8). Furthermore, $ZnWO_4$ photocatalysts present no visible light photocatalytic activity because of the large band gap (3.2 eV) but generate visible light after graphene hybidization, showing graphene is responsible for formation of the visible light performance, which is induced by the injection of an excited electron from the LUMO orbit of graphene to the CB of $ZnWO_4$.

Hybrid Structure and Optical Properties. Figure 3 shows the HRTEM images of $ZnWO_4$ and the $ZnWO_4$/graphene photocatalyst. As can be seen from Supporting Information Figure S1, the length of the $ZnWO_4$ nanorods is ∼1 μm, and the diameter is ∼30 nm. Figure 3a, b shows the HRTEM images of $ZnWO_4$ and the $ZnWO_4$/graphene photocatalyst. The photocatalysts exhibit the same interlayer spacing, 0.29 nm, corresponding to (111) crystal planes,

indicating there is no change in the lattice structure of $ZnWO_4$ after graphene is adsorbed onto the surface. As shown in Figure 3b, the lattice structure of $ZnWO_4$ is very orderly, and the outer boundary of the GZW0.2 sample is distinctly different from the core. The thickness of the graphene layer coats on the $ZnWO_4$ nanorods is estimated to be 0.747 nm, which is close to the scale of the monolayer chemically converted graphene (about 0.78 nm).[50,51]

The optical properties of the as-prepared samples were examined with UV−vis diffuse reflectance spectroscopy (Figure 4). As expected, $ZnWO_4$ exhibits its fundamental absorption
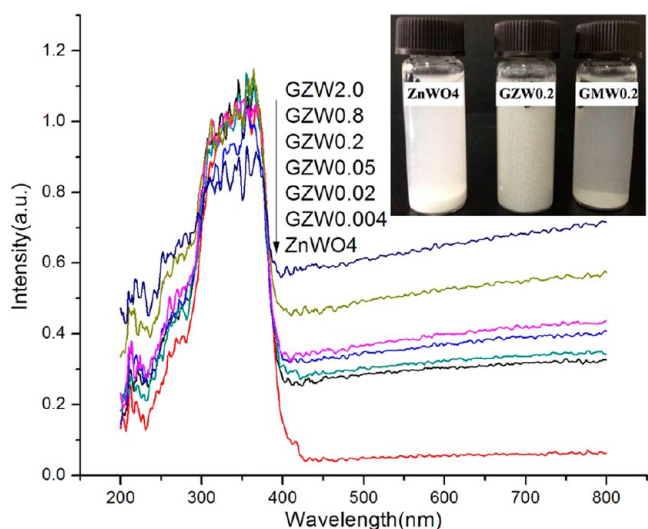

Figure 4. UV−vis diffuse reflection spectra of $ZnWO_4$ and $ZnWO_4$/graphene photocatalysts. The insert image displays the digital pictures of $ZnWO_4$, GZW0.2, and GMW0.2 suspensions.

sharp edge rising at 400 nm, whereas GZW0.2 shows absorption in the visible light region. Compared with $ZnWO_4$, the absorption edge of GZW0.2 experiences a red shift of about 20 nm. Moreover, it is noteworthy that there is an obvious positive correlation between the graphene content and the absorption intensity for all the GZW-X samples. This may be because introduction of the graphene can possibly cause

rapid separation of electron−hole pairs during irradiation.[52] The insert image displays the suspensions $ZnWO_4$, GZW0.2 and mixture GMW0.2. Clearly, GZW0.2 exhibits better dispersion than that of GMW0.2 with the same graphene contents. Good dispersion means chemical interaction force between $ZnWO_4$ and graphene, which is critical for photocatalytic process. This observation reveals a different interacting force between GZW0.2 and GMW0.2.

The photoluminescence (PL) emission and excitation spectra of as-prepared samples are shown in Figure 5a, b. It can be clearly seen that $ZnWO_4$ nanorods exhibit a blue emission band in the range of 400−550 nm, centered around 465 nm when excited by 286 nm, which agrees well with previous report for pristine $ZnWO_4$.[10] The spectral characteristics of $ZnWO_4$ are also very similar to some scheelite tungstate crystals (MWO_4, M = Pb, Ca, Ba).[53] The emission band shape may be explained by charge transfer transitions between the O_{2p} orbital and empty orbits of the central W_{5d} ions in the complex.[54] Indeed, the emission and excitation spectra displayed in Figure 5a, b clearly show that the addition of graphene quenches the fluorescence from the $ZnWO_4$ nanorods. The quenching mechanism of the PL spectra may be due to electron transfers from the excited $ZnWO_4$ nanorods. It may be possible to increase the rate of electron transfer and, thus, the interfacial interaction between the $ZnWO_4$ nanorods and graphene. Therefore, graphene is promising in enhancing the photocatalytic activity in terms of prolonging the electron−hole pair lifetime and accelerating the transfer rate of electrons.[27] Compared with the mixture GMW0.2, GZW0.2 shows decreased fluorescence intensity. The difference suggests an additional dominatong pathway for charge carriers to transport the photoinduced electron. Because of the interactions between the excited $ZnWO_4$ and graphene, as demonstrated earlier, such emission quenching represents interfacial charge-transfer processes.[55−58]

To further confirm this interaction, IR spectra were recorded for $ZnWO_4$ and $ZnWO_4$/graphene nanocomposites (see the Supporting Information Figure S4a, b, c). The vibrational peaks of GO are consistent with fingerprint groups such as carboxylic species, hydroxyl species, and epoxy species (C=O, 1734 cm^{-1}; OH deformation, 1400 cm^{-1}; the C−OH stretching, 1230 cm^{-1}; C−O−C stretching, 1061 cm^{-1}; skeletal ring
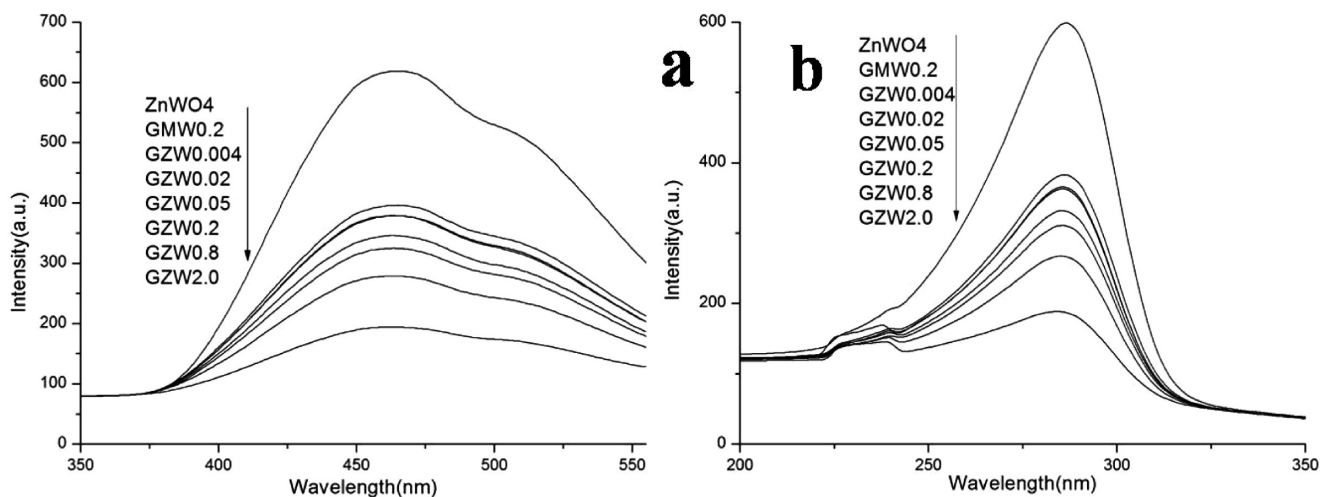

Figure 5. Room-temperature PL spectra of nanorod $ZnWO_4$ and $ZnWO_4$/graphene photocatalysts. (a) Emission spectra (λ_{ex} = 286 nm) and (b) excitation spectra (λ_{em} = 465 nm).

stretch, 1624 cm^{-1}).[59] The absorption band appearing at around 1580 cm^{-1} clearly shows the skeletal vibration of the graphene sheets, indicating the formation of a graphene structure.[33] The two peaks at 3447 and 1629 cm^{-1} observed for ZnWO$_4$ imply the existence of basic hydroxyl groups in the ZnWO$_4$ samples.[60] These results clearly indicate that the surface of ZnWO$_4$ is hydroxylated. Another IR peak at 1385 cm^{-1} results from the OH absorption of hydrogen-related defects.[61] The peak at 1385 cm^{-1} decreased and the peak at 1230 cm^{-1} (C−OH) is slightly observed for GZW0.2 (Supporting Information Figure S4c), indicating that defect sites may be occupied by graphene. The broad peak is located at 907 cm^{-1}, corresponding to the stretching W−O mode.[62] One peak for GZW0.2 shows a red shift around 437 cm^{-1}, which can be assigned to the stretching vibrations of the Zn−O bond.[63] Compared with GMW0.2, GZW0.2 shows a much broader peak around 1230 cm^{-1} (Supporting Information Figure S4a), which may be ascribed to the C−OH stretching originating from the characteristic peak of graphene. Thus, a supposition could be proposed that the graphene and ZnWO$_4$ are chemically bonded.

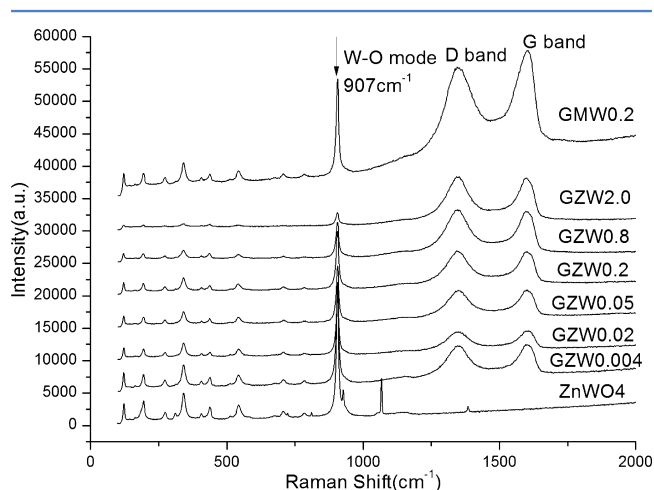Figure 6 shows the Raman spectra of graphene and the ZnWO$_4$/graphene composite. All the photocatalysts present the similar G and D band structure of carbon, which belongs to the characteristic peak of graphene. All GZW-X series samples exhibit two peaks around 1350 and 1600 cm^{-1}. The D band at around 1350 cm^{-1} is associated with the presence of surface defects in the graphitic layer.[34] In general, the I_D/I_G intensity ratio is a measure of disorder degree and average size of the sp^2 domains in graphite materials.[64] The increased I_D/I_G intensity ratio for GZW0.2 (I_D/I_G = 1.02) is observed relative to GMW0.2 (I_D/I_G = 0.95), indicating a decrease in the size of the in-plane sp^2 domains and the restablishment of the conjugated graphene network (sp^2 carbon). As shown in Figure 6, a higher intensity of the D band for GZW0.2 is observed, which means there may be more surface defects in GZW0.2 than in GMW0.2, whereas defects are a key influence factor for visible light absorption. Compared with graphene, the D band, slightly blue-shifted, and the G band, a little red-shift, are observed. These shifts could be attributed to the chemical interaction between ZnWO$_4$ and graphene.[36]

The X-ray diffraction (XRD) pattern of ZnWO$_4$/graphene photocatalysts prepared with different mass ratios of graphene to ZnWO$_4$ is shown in Supporting Information Figure S5. The ZnWO$_4$/graphene samples should present a two-phase composition: graphene and ZnWO$_4$ (JCPDS no.88-0251). No impurity phase is evident in the ZnWO$_4$/graphene samples. Notably, no typical diffraction peak belonging to the separate graphene is observed in the ZnWO$_4$/graphene nanocomposites. The reason can be ascribed to the fact that the main characteristic peak of graphene at 24.5° might be shielded by the main peak of ZnWO$_4$, which is at 24.5° and indexed to (110) crystal planes.[27]

To further investigate the interaction between ZnWO$_4$ and ZnWO$_4$/graphene, XPS spectra were carried out and are shown in Supporting Information Figure S6. The wide spectra (Supporting Information Figure S6a) of the ZnWO$_4$/graphene samples reveal the predominant presence of zinc, oxygen, tungsten, and carbon. The binding energy of W4f for GZW0.2 shows no change, as compared with the pure ZnWO$_4$ (Supporting Information Figure S6b). The XPS results reveal there was no change in the W environment or oxidation after hydrazine reduction.

Proposed Mechanism. In pricinple, specific surface, phase structure, and separation efficiency of photogenerated charges are crucial factors of photocatalytic activity. The BET surface
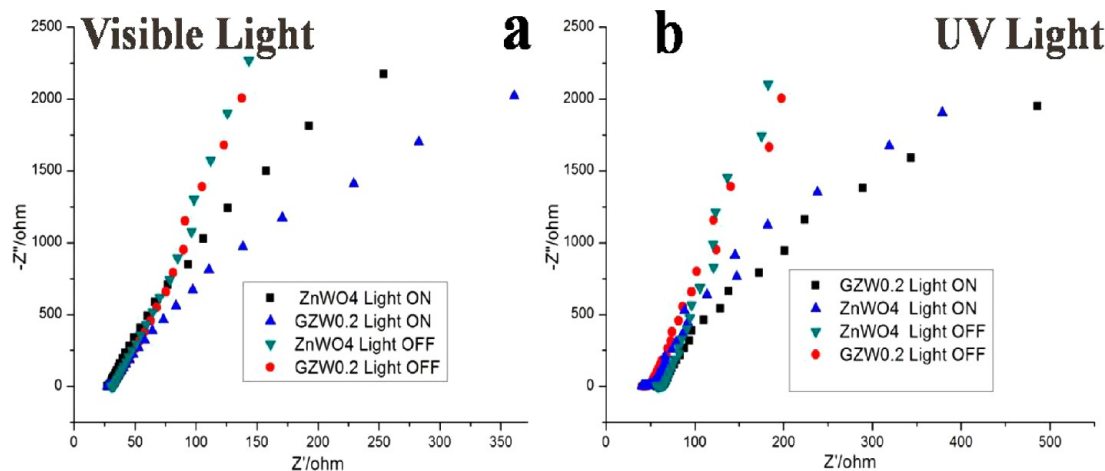

Figure 6. Raman spectra of ZnWO$_4$ and ZnWO$_4$/graphene photocatalysts.

Figure 7. Nyquist plots for ZnWO$_4$ and GZW0.2 in aqueous solution (a) in the dark and under visible light illumination and (b) in the dark and under UV light illumination [Na$_2$SO$_4$ = 0.1M].
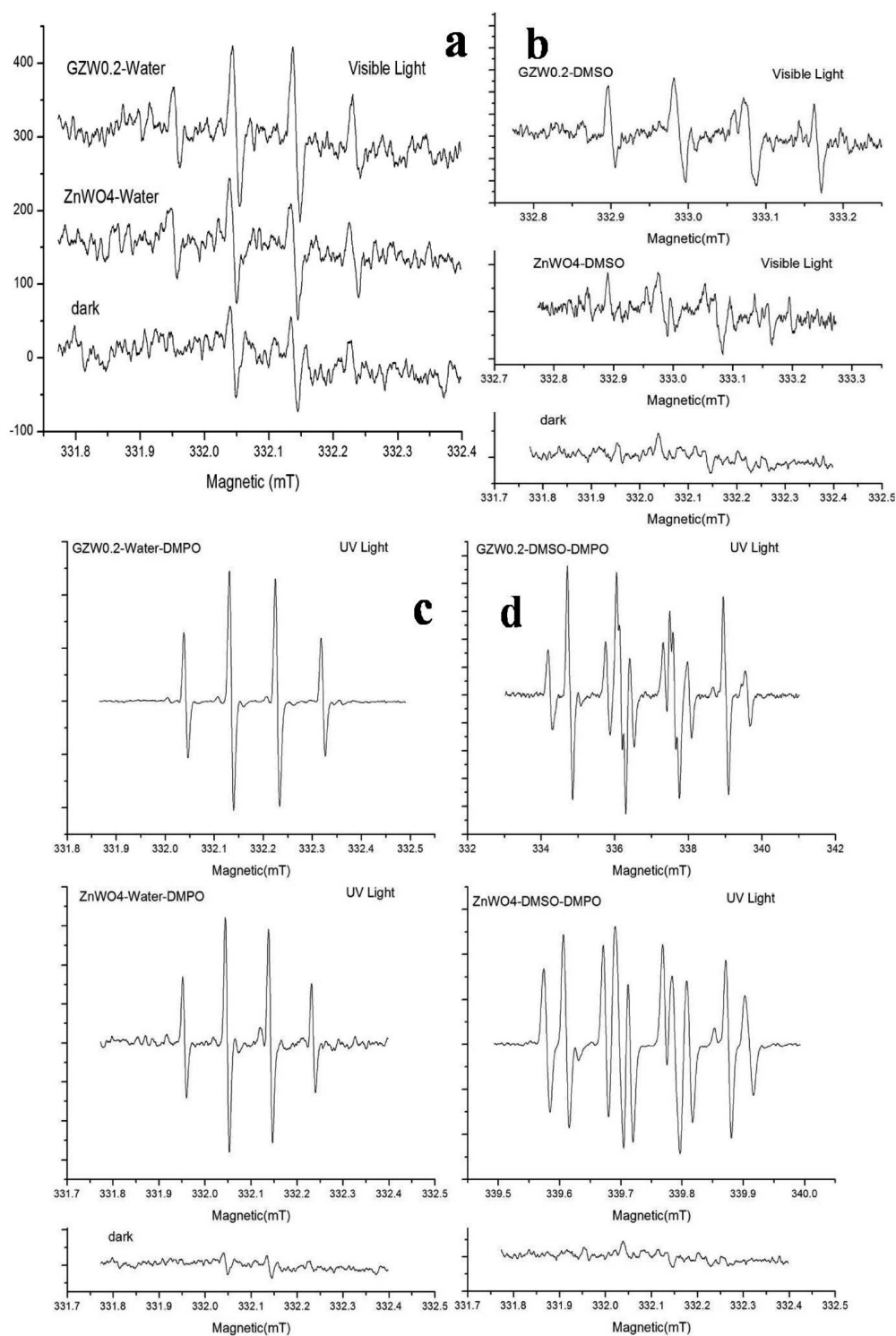
Figure 8. ESR spectra of $ZnWO_4$ and $ZnWO_4$/graphene photocatalysts in water and DMSO solvents (a, b) under visible light irradiation ($\lambda > 420$ nm) and (c, d) under UV light irradiation ($\lambda = 365$ nm) (DMPO as the radical trapper).

area of $ZnWO_4$ is $6.29 m^2/g$, and the BET surface area of $ZnWO_4$/graphene is $6.32 m^2/g$, showing no obvious changes. The dV/dD of $ZnWO_4$/graphene is ~29.6 nm and is ~16.2 nm for $ZnWO_4$ (Supporting Information Figure S3). The slight increase in dV/dD may be ascribed to graphene's loosing the stacking structure of the powder.[18] As discussed above, the BET surface area and the phase structure (Supporting Information Figure S5) of $ZnWO_4$/graphene remain almost

unchanged relative to $ZnWO_4$, indicating similar adsorption properties for both. Compared with that of pure $ZnWO_4$, GZW0.2 shows an enhanced adsorptivity (Supporting Information Figure S7). After adsorption equilibrium, 74.6% and 63.4% of MB remained in the solution, with pure $ZnWO_4$ and GZW0.2 photocatalyst, respectively. The enhancement of adsorption could be attributed to the $\pi-\pi$ stacking between MB and graphene.[20] Several approaches could be taken to
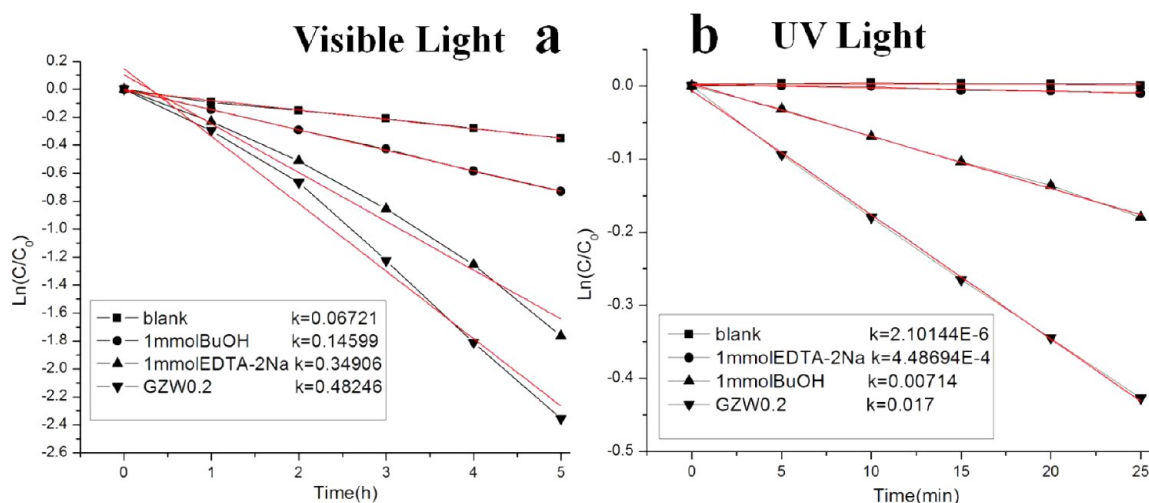
Figure 9. Apparent rate constants for the photocatalytic degradation of MB over GZW0.2 with the addition of hole and hydroxyl radical scavengers (a) under visible light irradiation ($\lambda > 420$ nm) and (b) under UV light irradiation light ($\lambda = 254$ nm).

improve the photocatalytic effiency, including enlarging the specific surface area, optimize the crystal structure, and accelerating the e−h separation rate for increasing the surface active site. Therefore, we believe that the enhancement of the photocatalytic activity of the $ZnWO_4$/graphene photocatalysts is attributed mainly to the effective separation of the photogenerated electron−hole pairs.

As previous studies, the photocatalytic reactions could be regarded as an electrochemical process.[40−42] Figure 7a, b shows electrochemical impedance spectra (EIS) Nyquist plots of $ZnWO_4$ and graphene/$ZnWO_4$ electrodes before and after light irradiation. This smaller arc radius implies a higher efficiency of charge transfer. The diameter of the arc radius for the GZW0.2 electrode is smaller than that for the $ZnWO_4$ electrode, regardless of UV or visible light irradiation. This result demonstrates that the introduction of graphene to $ZnWO_4$ can dramatically enhance the separation and transfer efficiency of photogenerated e−h pairs.

To confirm the mechanism further, ESR technique and trapping experiments of radicals were performed. ESR results are shown in Figure 8. Under visible light irradiation, much hydroxyl radical and little superoxide radical for $ZnWO_4$ and GZW0.2 samples in H_2O and DMSO are observed in Figure 8a, b. Meanwhile, hydroxyl and superoxide radicals under UV light irradiation appear (Figure 8c, d) for $ZnWO_4$ and GZW0.2 samples in H_2O and DMSO solvents, respectively. The signal for GZW0.2 is stronger than that in $ZnWO_4$, thus accounting for the higher photocatalytic performance of GZW0.2 than the bare $ZnWO_4$ toward the degradation of pollutants.

Furthermore, the signal of the carbon free radical was found in the $ZnWO_4$ and GZW0.2 suspension in the presence of DMSO under visible and UV light irradiation (Figure 8d), and the intensity for GZW0.2 is stronger than that for $ZnWO_4$. The carbon free radical plays a decisive role in stabling and prolonging the lifetime of other active and oxidative radicals ($^\bullet OH$ and $O_2^{\bullet-}$), although it has no activity for degradation of pollutants. The carbon free radical derives from the defects structure of the graphene film in $ZnWO_4$/graphene. Thus, the enhanced photocatalytic activity of GZW0.2 compared with $ZnWO_4$ is due mainly to the larger amount and longer lifetime of oxidative radicals ($^\bullet OH$ and $O_2^{\bullet-}$) which enriched and prolonged by the more stable carbon free radical.

Figure 9 shows the photodegradation of MB with the addition of a hydroxyl radical scavenger (tBuOH)[65] and hole scavenger (EDTA-2Na)[66] under visible and UV light irradiation, respectively. Under visible light irradiation, as shown in Figure 9a, the photocatalytic activity of GZW0.2 decreases slightly by the addition of hole scavengers (EDTA-2Na) and reduces largely with the addition of hydroxyl radical scavengers, indicating that the holes are not the main oxidative species for GZW0.2 samples. That is, the hydroxyl radical mainly governs the visible light photocatalytic process. However, the result is reversed under UV light irradiation, as shown in Figure 9b, indicating that the holes are the main active species. It is proven that the photocatalytic mechanism under UV and visible light irradiation may be different.

The separation and transportation of electron−hole pairs at the interface of $ZnWO_4$/graphene photocatalysts is proposed in Scheme 1. $ZnWO_4$ can absorb light to produce photogenerated electron−hole pairs. Since the VB position of $ZnWO_4$ is lower than the HOMO orbit of graphene, the photogenerated holes on $ZnWO_4$ could transfer easily to graphene via the well developed interface. Meanwhile, the CB position of $ZnWO_4$ is lower than the LUMO orbit of graphene, and the photogenerated electrons on graphene can directly inject to the CB band of $ZnWO_4$, making the charge separation more efficient and reducing the probability of recombination, thus resulting in an enhanced photocatalytic activity. As shown in Scheme 1a, the high separation efficiency of photoinduced electron−hole pairs is supposed to be responsible for the enhanced UV light photocatalytic activity, resulting in the increase in the number of holes participated in the photooxidation process. As shown in Scheme 1b, the enhancement of visible light performance is induced by the injection of an excited electron from the LUMO orbit of graphene to the CB of $ZnWO_4$. These electrons could easily migrate from the inner region to the surface to take part in the surface reaction to form radicals ($^\bullet OH$ and $O_2^{\bullet-}$) which are prolonged and enriched by the more stable carbon free radical derived from graphene, thus dramatically producing visible light activity. This effective separation of photogenerated electron−hole pairs driven by band potentials between two components is also reported in other systems, such as C_3N_4/ZnO,[20] C_3N_4/BiPO$_4$,[67] and C_3N_4/TaON.[68] The proposition is consistent with PL spectra (Figure 5), in which $ZnWO_4$/

Scheme 1. Schematic Drawing Illustrating the Mechanism of Charge Separation and Photocatalytic Process over ZnWO$_4$/Graphene Photocatalysts under UV Light (a) and Visible Light (b) Irradiation
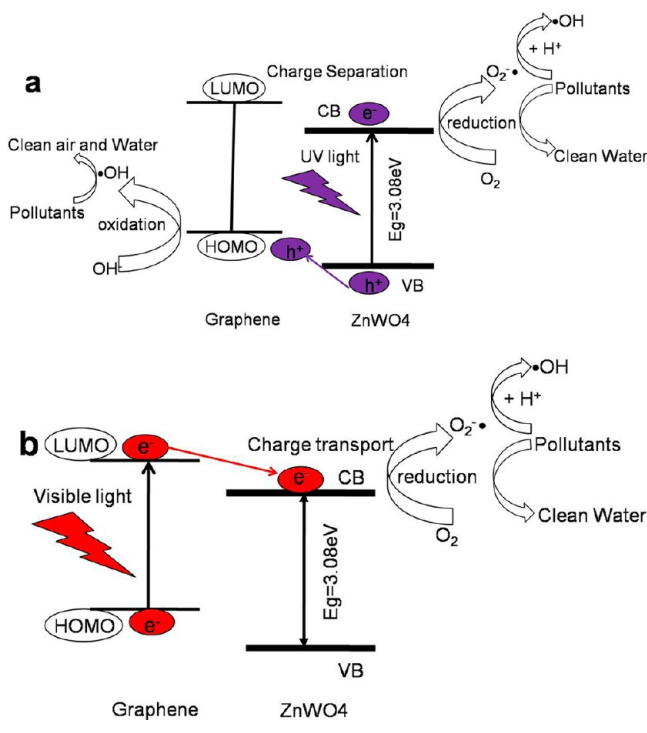
graphene samples show significant reduced excitation compared with ZnWO$_4$, suggesting the inhibited recombination of excited electron−hole pairs. In the view of this point, the enhancement of photocatalytic activity for GZW0.2 should be attributed to the migration effect of photoinduced electrons on the interface of graphene and ZnWO$_4$.

Furthermore, this high separation efficiency may be not only due to the heterojunction interfaces, but also due to the anisotropic growth of ZnWO$_4$, in which the long aspect ratio provides a sufficiently spacious transport channel for charge separation, as demonstrated in other nanoribbon structures, such as Zn$_2$GeO$_4$.[69]

CONCLUSIONS

Graphene-hybridized ZnWO$_4$ photocatalysts were synthesized via a facile in situ reduction reaction. Visible light photocatalytic activity was produced, and the UV photocatalytic activity was 2.3 times that of pristine ZnWO$_4$ after ZnWO$_4$ hybridized by graphene (GZW0.2). The formation of visible light performance is induced by the injection of an excited electron from the LUMO orbit of graphene to the CB of ZnWO$_4$ due to its photosensitization. The enhancement of UV light photocatalytic activity resulted from the high separation efficiency of photoinduced electron−hole pairs promoted via graphene hybridization. This work can provide important inspirations for developing of graphene hybridized materials.

ASSOCIATED CONTENT

Ⓢ Supporting Information

Synthesis details of graphene oxide and graphene, BET curves, TEM images of ZnWO$_4$ and GZW0.2, FTIR spectra, XRD patterns, XPS spectra of ZnWO$_4$ and ZnWO$_4$/graphene, and adsorption curves of ZnWO$_4$ and GZW0.2. This information is available free of charge via the Internet at http://pubs.acs.org/.

AUTHOR INFORMATION

Corresponding Author
*Phone: +86-10-62787601. Fax: +86-10-62787601. E-mail: zhuyf@tsinghua.edu.cn.

Notes
The authors declare no competing financial interest.

ACKNOWLEDGMENTS

REFERENCES

(1) Kudo, A.; Omori, K.; Kato, H. *J. Am. Chem. Soc.* **1999**, *121*, 1145−1155.
(2) Asahi, R.; Morikawa, T.; Ohwaki, T.; Aoki, K.; Taga, Y. *Science* **2001**, *293*, 269−271.
(3) Zou, Z. G.; Ye, J. H.; Sayama, K.; Arakawa, H. *Nature* **2001**, *414*, 625−627.
(4) Zhang, L. W.; Zhu, Y. F. *Catal. Sci. Technol.* **2012**, *2*, 694−706.
(5) Hoffmann, M.; Martin, S.; Choi, W. *Chem. Rev.* **1995**, *95*, 69−96.
(6) Fu, H. B.; Lin, J.; Zhang, L. W.; Zhu, Y. F. *Appl. Catal., A* **2006**, *306*, 58−67.
(7) Zhao, X.; Zhu, Y. F. *Environ. Sci. Technol.* **2006**, *40*, 3367−3372.
(8) Lin, J.; Lin, J.; Zhu, Y. F. *Inorg. Chem.* **2007**, *46*, 8372−8378.
(9) Bonanni, M.; Spanhel, L.; Lerch, M.; Fuglein, E.; Muller, G. *Chem. Mater.* **1998**, *10*, 304−310.
(10) Huang, G. L.; Zhang, C.; Zhu, Y. F. *J. Alloys Compd.* **2007**, *432*, 269−276.
(11) Lin, J.; Lin, J.; Zhu, Y. F. *Inorg. Chem.* **2007**, *46*, 8372−8378.
(12) Liu, B.; Yu, S. H.; Li, L. J.; Zhang, F.; Zhang, Q.; Yoshimura, M.; Shen, P. K. *J. Phys. Chem. B* **2004**, *108*, 2788−2792.
(13) Huang, G. L.; Zhu, Y. F. *J. Phys. Chem. C* **2007**, *111*, 11952−11958.
(14) Chen, S. H.; Sun, S. X.; Sun, H. G.; Fan, W. L.; Zhao, X.; Sun, X. *J. Phys. Chem. C* **2010**, *114*, 7680−7688.
(15) Zhang, H. J.; Chen, G. H.; Bahnemann, D. W. *J. Mater. Chem.* **2009**, *19*, 5089−5121.
(16) He, D. Q.; Wang, L. L.; Xu, D. D.; Zhai, J. L.; Wang, D. J.; Xie, T. F. *ACS Appl. Mater. Interfaces* **2011**, *3*, 3167−3171.
(17) Sun, L. M.; Zhao, X.; Cheng, X. F.; Sun, H. G.; Li, Y. L.; Li, P.; Fan, W. L. *J. Phys. Chem. C* **2011**, *115*, 15516−15524.
(18) Fu, H. B.; Xu, T. G.; Zhu, S. B.; Zhu, Y. F. *Environ. Sci. Technol.* **2008**, *42*, 8064−8069.
(19) Zhang, H.; Zhu, Y. F. *J. Phys. Chem. C* **2010**, *114*, 5822−5826.
(20) Wang, Y. J.; Shi, R.; Lin, J.; Zhu, Y. F. *Environ. Sci. Technol.* **2011**, *4*, 2922−2929.
(21) Wang, Y. J.; Bai, X. J.; Pan, C. S.; He, J.; Zhu, Y. F. *J. Mater. Chem.* **2012**, *22*, 11568−11573.
(22) Zhao, L.; Chen, X. F.; Wang, X. C.; Zhang, Y. J.; Wei, W.; Sun, Y. H.; Antonietti, M.; Titirici, M. M. *Adv. Mater.* **2010**, *22*, 3317−3321.
(23) Yang, S. B.; Feng, X. L.; Wang, X. C.; Mullen, K. *Angew. Chem., Int. Ed.* **2011**, *50*, 5339−5343.
(24) Zhang, Y. H.; Tang, Z. R.; Fu, X. Z.; Xu, Y. J. *ACS Nano* **2010**, *4*, 7303−7314.
(25) Geim, A. K.; Novoselov, K. S. *Nat. Mater.* **2007**, *6*, 183−191.
(26) Zhang, Y.; Tan, Y.; Stormer, H. L.; Kim, P. *Nature* **2005**, *438*, 201−204.
(27) Zhang, Y. H.; Tang, Z. R.; Fu, X. Z.; Xu, Y. J. *ACS Nano* **2010**, *4*, 7303−7314.

(28) Williams, G.; Seger, B.; Kamat, P. V. *ACS Nano* **2008**, *2*, 1487−1491.

(29) Williams, G.; Kamat, P. V. *Langmuir* **2009**, *25*, 13869−13873.

(30) Lee, J. M.; Pyun, Y. B.; Yi, J.; Choung, J. W.; Park, W. I. *J. Phys. Chem. C* **2009**, *113*, 19134−19138.

(31) Schaetz, A.; Zeltner, M.; Stark, W. J. *ACS Catal.* **2012**, *2*, 1267−1284.

(32) Min, S. X.; Lu, G. X. *J. Phys. Chem. C* **2011**, *115*, 13938−13945.

(33) Zhang, H.; Lv, X. J.; Li, Y. M.; Wang, Y.; Li, J. H. *ACS Nano* **2010**, *4*, 380−386.

(34) Fu, Y. S.; Wang, X. *Ind. Eng. Chem. Res.* **2011**, *50*, 7210−7218.

(35) Ng, Y. H.; Iwase, A.; Kudo, A.; Amal, R. *J. Phys. Chem. Lett.* **2010**, *1*, 2607−2612.

(36) Xu, T. G.; Zhang, L. W.; Cheng, H. Y.; Zhu, Y. F. *Appl. Catal., B* **2011**, *101*, 382−387.

(37) Hummers, W. S.; Offeman, R. E. *J. Am. Chem. Soc.* **1958**, *80*, 1339−1339.

(38) Nethravathi, C.; Rajamathi, M. *Carbon* **2008**, *46*, 1994−1998.

(39) Li, D.; Muller, M. B.; Gilje, S.; Kaner, R. B.; Wallace, G. G. *Nat. Nanotechnol.* **2008**, *3*, 101−105.

(40) Liu, H.; Cheng, S.; Wu, M.; Wu, H.; Zhang, J.; Li, W.; Cao, C. *J. Phys. Chem. A* **2000**, *104*, 7016−7020.

(41) Leng, W. H.; Zhang, Z.; Zhang, J. Q.; Cao, C. N. *J. Phys. Chem. B* **2005**, *109*, 15008−15023.

(42) Park, H.; Choi, W. *J. Phys. Chem. B* **2003**, *107*, 3885−3890.

(43) Akhavan, O.; Abdolahad, M.; Esfandiar, A.; Mohatashamifar, M. *J. Phys. Chem. C* **2010**, *114*, 12955−12959.

(44) Akhavan, O. *ACS Nano* **2010**, *4*, 4174−4180.

(45) Li, Z.; Zhang, W.; Luo, Y.; Yang, J.; Hou, J. G. *J. Am. Chem. Soc.* **2009**, *131*, 6320−6321.

(46) Gaya, U. I.; Abdullah, A. H. *J. Photochem. Photobiol. C* **2008**, *9*, 1−12.

(47) Kuo, T. J.; Lin, C. N.; Kuo, C. L.; Huang, M. H. *Chem. Mater.* **2007**, *19*, 5143−5147.

(48) Akhavan, O.; Choobtashani, M.; Ghaderi, E. *J. Phys. Chem. C* **2012**, *116*, 9653−9659.

(49) Wang, W. S.; Wang, D. H.; Qu, W. G.; Lu, L. Q.; Xu, A. W. *J. Phys. Chem. C* **2012**, *116*, 19893−19901.

(50) Fan, X.; Peng, W.; Li, Y.; Li, X.; Wang, S.; Zhang, G.; Zhang, F. *Adv. Mater.* **2008**, *20*, 4490−4493.

(51) Li, D.; Muller, M. B.; Gilje, S.; Kaner, R. B.; Wallace, G. G. *Nat. Nanotechnol.* **2008**, *3*, 101−105.

(52) Zhang, L. W.; Fu, H. B.; Zhu, Y. F. *Adv. Funct. Mater.* **2008**, *18*, 2180−2189.

(53) Nikl, M.; Bohacek, P.; Mihokova, E.; Kobayashi, M.; Ishii, M.; Usuki, Y.; Babin, V.; Stolovich, A.; Zazubovich, S.; Bacci, M. *J. Lumin.* **2000**, *87*, 1136−1139.

(54) Wang, H.; Medina, F. D.; Liu, D. D.; Zhou, Y. D. *J. Phys.: Condens. Matter.* **1994**, *6*, 5373−5386.

(55) Chen, Z.; Berciaud, S.; Nuckolls, C.; Heinz, T. F.; Brus, L. E. *ACS Nano* **2010**, *4*, 2964−2968.

(56) Kamat, P. V.; Patrick, B. *J. Phys. Chem.* **1992**, *96*, 6829−6834.

(57) Subramanian, V.; Wolf, E. E.; Kamat, P. V. *J. Phys. Chem. B* **2003**, *107*, 7479−7485.

(58) Kamat, P. V.; Huehn, R.; Nicolaescu, R. *J. Phys. Chem. B* **2002**, *106*, 788−794.

(59) Xu, Y.; Bai, H.; Lu, G.; Li, C.; Shi, G. *J. Am. Chem. Soc.* **2008**, *130*, 5856−5857.

(60) Gotic, M.; Ivanda, M.; Popovic, S.; Music, S. *Mater. Sci. Eng., B* **2000**, *B77*, 193−201.

(61) Li, Z. S.; Yu, T.; Zou, Z. G.; Ye, J. H. *Appl. Phys. Lett.* **2006**, *88*, 071917−(1-3).

(62) Kalinko, A.; Kuzmin, A. *J. Lumin.* **2009**, *129*, 1144−1147.

(63) Wang, J. C.; Liu, P.; Fu, X. Z.; Li, Z. H.; Han, W.; Wang, X. X. *Langmuir* **2009**, *25*, 1218−1223.

(64) Gómez-Navarro, C.; Weitz, R. T.; Bittner, A. M.; Scolari, M.; Mews, A.; Burghard, M.; Kern, K. *Nano Lett.* **2007**, *7*, 3499−3503.

(65) Lee, H.; Choi, W. *Environ. Sci. Technol.* **2002**, *36*, 3872−3878.

(66) Zhou, J. H.; Deng, C. Y.; Si, S. H.; Shi, Y.; Zhao, X. L. *Electrochim. Acta* **2011**, *56*, 2062−2067.

(67) Pan, C. S.; Xu, J.; Wang, Y. J.; Li, D.; Zhu, Y. F. *Adv. Funct. Mater.* **2012**, *22*, 1518−1524.

(68) Yan, S. C.; Lv, S. B.; Li, Z. S.; Zou, Z. G. *Dalton Trans.* **2010**, *39*, 1488−1491.

(69) Liu, Q.; Zhou, Y.; Kou, J. H.; Chen, X. Y.; Tian, Z. P.; Gao, J.; Yan, S. C.; Zou, Z. G. *J. Am. Chem. Soc.* **2010**, *132*, 14385−14387.